

# Paleoceanography and Paleoclimatology

## RESEARCH ARTICLE

10.1029/2020PA004084

### Key Points:

- We present organic geochemical records of water temperature and primary productivity (1.4–0.3 Million years) from the Agulhas Plateau
- Our data indicate the Subtropical Front was south of the Agulhas Plateau during the mid-Pleistocene Interim State (0.9–0.47 Ma)
- Only the most extreme northward migrations of the Subtropical Front are associated with Agulhas leakage reductions

### Supporting Information:

Supporting Information may be found in the online version of this article.

### Correspondence to:

A. Cartagena-Sierra,  
[acartage@nd.edu](mailto:acartage@nd.edu)

### Citation:

Cartagena-Sierra, A., Berke, M. A., Robinson, R. S., Marcks, B., Castañeda, I. S., Starr, A., et al. (2021). Latitudinal migrations of the Subtropical Front at the Agulhas Plateau through the mid-Pleistocene Transition. *Paleoceanography and Paleoclimatology*, 36, e2020PA004084. <https://doi.org/10.1029/2020PA004084>

Received 30 AUG 2020

Accepted 13 APR 2021

## Latitudinal Migrations of the Subtropical Front at the Agulhas Plateau Through the Mid-Pleistocene Transition

Alejandra Cartagena-Sierra<sup>1</sup> , Melissa A. Berke<sup>1</sup> , Rebecca S. Robinson<sup>2</sup> , Basia Marcks<sup>2</sup>, Isla S. Castañeda<sup>3</sup> , Aidan Starr<sup>4</sup> , Ian R. Hall<sup>4</sup> , Sidney R. Hemming<sup>5</sup>, Leah J. LeVay<sup>6</sup> , and Expedition 361 Scientific Party<sup>7</sup>

<sup>1</sup>Department of Civil & Environmental Engineering & Earth Sciences, University of Notre Dame, Notre Dame, IN, USA,

<sup>2</sup>Graduate School of Oceanography, University of Rhode Island, Narragansett, RI, USA, <sup>3</sup>Department of Geosciences, University of Massachusetts Amherst, Amherst, MA, USA, <sup>4</sup>School of Earth Sciences, Cardiff University, Cardiff, UK,

<sup>5</sup>Department of Earth and Environmental Sciences and Lamont-Doherty Earth Observatory of Columbia University, Palisades, NY, USA, <sup>6</sup>International Ocean Discovery Program, Texas A&M University, College Station, TX, USA, <sup>7</sup>See Supporting Information S1

**Abstract** The meridional variability of the Subtropical Front (STF) in the Southern Hemisphere, linked to expansions or contractions of the Southern Ocean, may have played an important role in global ocean circulation by moderating the magnitude of water exchange at the Indian-Atlantic Ocean Gateway, so called Agulhas Leakage. Here we present new biomarker records of upper water column temperature ( $U_{37}^K$  and  $TEX_{86}$ ) and primary productivity (chlorins and alkenones) from marine sediments at IODP Site U1475 on the Agulhas Plateau, near the STF and within the Agulhas retroflection pathway. We use these multiproxy time-series records from 1.4 to 0.3 Ma to examine implied changes in the upper oceanographic conditions at the mid-Pleistocene transition (MPT, ca. 1.2–0.8 Ma). Our reconstructions, combined with prior evidence of migrations of the STF over the last 350 ka, suggest that in the Southwestern Indian Ocean the STF may have been further south from the Agulhas Plateau during the mid-Pleistocene Interim State (MPIS, MIS 23–12) and reached its northernmost position during MIS 34–24 and MIS 10. Comparison to a *Globorotalia menardii*-derived Agulhas Leakage reconstruction from the Cape Basin suggests that only the most extreme northward migrations of the STF are associated with reduced Agulhas Leakage. During the MPIS, STF migrations do not appear to control Agulhas Leakage variability, we suggest previously modeled shifting westerly winds may be responsible for the patterns observed. A detachment between STF migrations and Agulhas Leakage, in addition to invoking shifting westerly winds may also help explain changes in CO<sub>2</sub> ventilation seen during the MPIS.

## 1. Introduction

The upper water column south of Africa is a complex intersection of the Agulhas System and the Subtropical Front (STF), and it comprises a triple boundary between the Atlantic, Indian, and Southern Oceans (Figure 1). As a consequence, it has been suggested that this region plays a critical role in regulating global climate (Gordon, 2003). Within the Agulhas System in the Southwest Indian Ocean, the Agulhas Current (AC) is fed by surface and thermocline waters from the Red and Arabian Seas, the Indonesian Throughflow, the Mozambique Channel, and the East Madagascar Current (Beal et al., 2006). The AC transports these surface waters southward along the southeast coast of Africa and once it reaches the southern tip of South Africa, it is retroflected into the Indian Ocean by the westerly winds (Lutjeharms, 2006) and continues to flow eastward as the Agulhas Return Current (ARC) (Lutjeharms & Ansoorge, 2001). A portion of the salty, warm waters transported by the AC leaks into the Atlantic Ocean. It has been suggested that temperature and salinity variability of the AC has an impact not only on southern Africa, but also around the Atlantic Ocean (Beal et al., 2011). The STF forms the northernmost border of the Southern Ocean Frontal system and delimits the southern extent of the Agulhas System (Figure 1). This hydrographic boundary is currently located at ~39–41°S and separates the colder, nutrient-rich Subantarctic Zone waters from the warm, salty, and nutrient-poor subtropical waters (Orsi et al., 1995; Stramma & Peterson, 1990). It generally exhibits a mean temperature range of 10.6–17.9°C (Lutjeharms & Valentine, 1984). South of Africa, the STF sits to the south of the Agulhas Plateau, while retroflected Agulhas waters become the ARC in the northern side of the Agulhas Plateau due to bathymetrical steering (Lutjeharms, 2006). South of the STF, the Subantarctic Zone

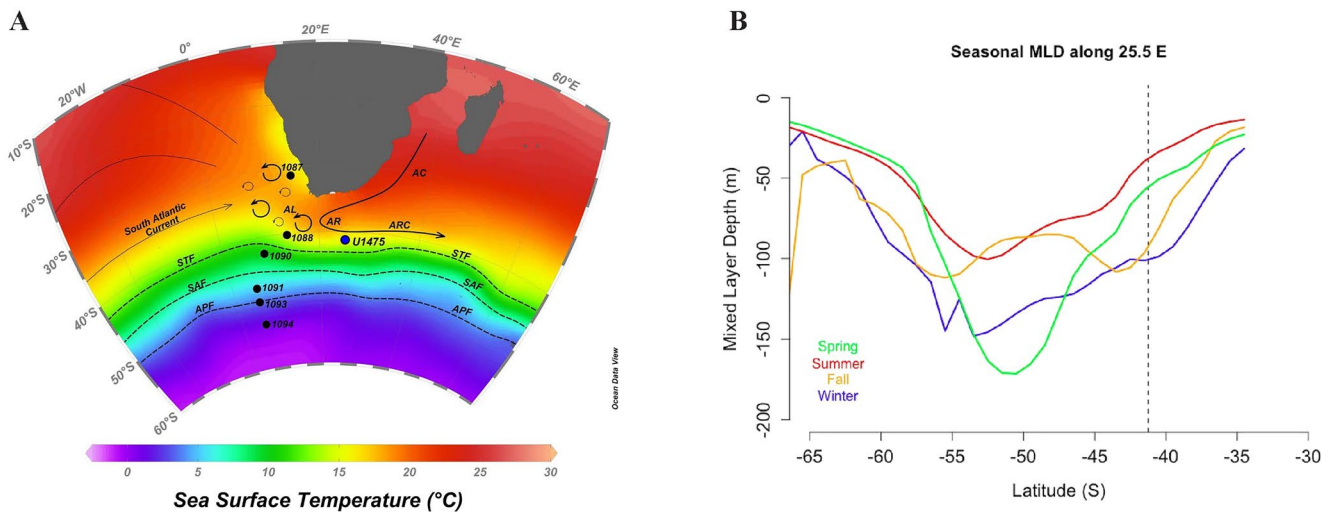


**Figure 1.** Map of the location of International Ocean Discovery Program (IODP) Site U1475 and nearby sites used for comparison. (a) sea surface temperatures map displaying schematic pathways of the Agulhas Current, Agulhas Leakage, Agulhas Retroflection, Agulhas Retroflection Current, Subtropical Front, and Subantarctic front. Location of IODP Site U1475 (blue circle) and nearby sites (black circles) are also shown, and dashed lines represent approximate locations of oceanic frontal zones. (b) Seasonal mixed layer depth along 25.5°E based on Monterey and Levitus (1997). Dashed vertical line shows the location of Site U1475.

(SAZ) is located between the STF and the Subantarctic Front (SAF). The SAF is the northernmost edge of the Antarctic Circumpolar Current (ACC) and separates the SAZ from the Polar Frontal Zone. South of the SAF, the Antarctic Polar Front (APF) acts as the hydrographic boundary dividing the Polar Frontal Zone and the Antarctic Zone waters transported by the ACC (Belkin & Gordon, 1996; Orsi et al., 1995; Pollard et al., 2002; Whitworth & Nowlin, 1987).

The Agulhas System is considered a key player in global meridional overturning circulation due to its important role in the inter-ocean exchange of warm, saline waters between the Indian and Atlantic Oceans via Agulhas Leakage (Beal et al., 2011; Gordon, 2003; Lutjeharms, 2006; Weijer, 2002). Changes in the latitudinal position of the STF have been postulated to influence the amount of Agulhas Leakage (Bard & Rickaby, 2009; Beal et al., 2011; Becquey & Gersonde, 2002; Caley et al., 2012; Schefuß et al., 2004; Simon et al., 2013), with climate repercussions over a range of timescales (Beal et al., 2011; Martínez-Méndez et al., 2010). Northern migrations of the STF and nutrient-rich SAZ waters during the glacial periods of the last 150 kyr are inferred from increases in surface water productivity and cooler temperatures within the ARC (Naik et al., 2013). Northward displacements of the STF during glacial periods are also evident in changes in diatom assemblages, bulk biogenic silica content, and alkenone-based sea surface temperatures (SST) over the last 350 kyr at the Agulhas Plateau (Romero et al., 2015). In the southeast Atlantic, changes in foraminiferal assemblages have been associated with warm Agulhas waters leaking through the Indian-Atlantic Ocean Gateway (Caley et al., 2012; Peeters et al., 2004). Thus, changes in the abundances of Agulhas Leakage fauna in the southeast Atlantic have been interpreted as a proxy of Agulhas Leakage, which have also been related to latitudinal migrations of the STF during the Quaternary (Caley et al., 2012; Peeters et al., 2004).

The MPT marks the Quaternary climate transition between 41 kyr to more intense 100 kyr glacial-interglacial cycles (Berger & Jansen, 1994; Clark et al., 2006; Hodell et al., 2008; Raymo et al., 1997). The MPT also witnessed dramatic changes in intermediate and deep water temperatures, and associated extinctions of benthic foraminifers (Hayward et al., 2007; O'Neill et al., 2007). The onset of the MPT is often credited as a response to the long-term cooling trend, possibly induced by decreasing atmospheric CO<sub>2</sub> crossing an internal system threshold (Berger & Jansen, 1994; Raymo et al., 1997). However, other proposed explanations point to changes in ice-sheet dynamics (Clark & Pollard, 1998; Clark et al., 2006; Raymo et al., 2006; Pollard & DeConto, 2009). Changes in overturning and sea ice extent have been implicated in carbon cycle changes at the MPT, with potential linkages to the extent of the Southern Ocean or Agulhas Leakage (Becquey & Gersonde, 2002; Kemp et al., 2010; Lear et al., 2016; Martínez-García et al., 2011).

Multiple approaches have been taken to define the MPT (Clark et al., 2006; Elderfield et al., 2012; McClymont et al., 2013; Raymo et al., 1997). Here, we discuss the MPT in terms of the: (a). “900-kyr event,” (b). “mid-Pleistocene Interim State” (MPIS), and (c). “Mid-Brunhes Event” (MBE), which broadly mark two major steps and the termination of the MPT, respectively (Clark et al., 2006; Elderfield et al., 2012; McClymont et al., 2013). The “900-kyr event” (MIS 24–22) marks the end or reduction of the long-term cooling trend (McClymont et al., 2013) that began during the Pliocene (Ravelo et al., 2004). This event includes cool interglacial MIS 23, the only known interglacial period where the Atlantic meridional overturning circulation (AMOC) did not strengthen (Dausmann et al., 2017; Peña & Goldstein, 2014), and has been suggested to mark the crossing of a climate threshold (McClymont et al., 2013). Following the 900-kyr event, the interval known as the MPIS, spanning from MIS 22 to the onset of MIS 13, is a period of generally reduced overturning circulation (Kemp et al., 2010; Schmieder et al., 2000). Evidence of reduced carbonate burial, likely due to dissolution, comes from records of elevated magnetic susceptibility and reduced sedimentation rates in the South Atlantic (Schmieder et al., 2000). Records from ODP Site 1090 in the South Atlantic SAZ (42°54.8'S, 8°53.9'E, 3,700 m, Figure 1) show temperatures and changes in the foraminiferal community that suggest a northward migration of the SAF to a location near Site 1090 during the MPIS (Becquey & Gersonde, 2002; Martínez-García et al., 2009). The last significant climatic event during the MPT is the MBE, which is characterized by an increase in ice volume variability (Lisiecki & Raymo, 2005), interglacial intervals with warmer temperatures (Elderfield et al., 2012; Jouzel et al., 2007; Lawrence et al., 2009) and a higher concentrations of atmospheric CO<sub>2</sub> (Hönisch et al., 2009; Lüthi et al., 2008). This event occurred during glacial termination V (T5) at around 424 ka (Jansen et al., 1986) and coincided with an increase in the mean flow speed of the Deep Western Boundary Current and likely intensification of Antarctic Bottom Water formation and export (Hall et al., 2001).

Significant latitudinal migrations of Southern Ocean fronts have been suggested for the MPT for sites in the South Atlantic (Becquey & Gersonde, 2002; Kemp et al., 2010). Kemp et al. (2010) proposed that the MPT is marked by the beginning of stepwise northward migration of the APF. The first northward movement of the APF is defined by the disappearance of the laminated diatom mats at the Site 1093 (49°58.6'S, 5°51.9'E, 3,626 m water depth) and appearance at Site 1091 (47°5.7'S, 5°55.2'E, 4,363 m water depth) during the 900-kyr event (Figure 1a). A second, and even greater equatorward migration of the APF is inferred from the disappearance of the laminated diatom mats at Site 1091 (Kemp et al., 2010) and associated cooling in the Subantarctic Zone of the South Atlantic (Becquey & Gersonde, 2002) during the MPIS. The laminated diatom mats return to their southernmost position during the MBE, indicating that the APF was proximally located to Site 1094 (53°10.8'S, 5°7.8'E, 2,806 m water depth). While the evidence for movement of the ACC fronts in the Atlantic seems strong, there is no clear evidence that the STF migrated north and expanded the Southern Ocean, during the MPIS (Kemp et al., 2010).

Northward expansions of the Southern Ocean fronts, including the STF, have been proposed to limit the amount of warm and salty water escaping from the Indian Ocean into the South Atlantic through Agulhas Leakage. This study aims to examine oceanographic changes within the upper (~50–200 m) water column at the Agulhas Plateau through the MPT. To investigate latitudinal changes of the STF in the Southwestern Indian Ocean, we produced a multiproxy reconstruction from 1.4 to 0.3 Ma of primary productivity and upper water column temperature using sediments from Site U1475 at the Agulhas Plateau from IODP Expedition 361. Past water temperature is estimated using the  $U_{37}^K$  and  $TEX_{86}$  paleotemperature indices (Brassell et al., 1986; Schouten et al., 2002). The  $U_{37}^K$  index is based on the analysis of the di- and tri-unsaturated alkenones synthesized by unicellular haptophyte marine algae (Eglinton & Eglinton, 2008; Volkman et al., 1980). The  $TEX_{86}$  index is based on the analysis of glycerol dialkyl glycerol tetraethers (GDGTs) with 86 carbon atoms, membrane lipids produced by Thaumarchaeota (Brochier-Armanet et al., 2008). GDGT producers are thought to be chemoautotrophic nitrifiers that could live within the upper water column (~50–200 m) (Karner et al., 2001; Könneke et al., 2005), and therefore might reflect water masses temperatures below the surface (Huguet et al., 2007). Upper water column productivity variations are reconstructed using chlorins and total  $C_{37:3-2}$  alkenone abundances (Harris et al., 1996; Volkman et al., 1980). Chlorins are diagenetic products of chlorophyll, and thus changes in their abundances represent changes in primary productivity of the total phytoplankton community (Harris et al., 1996). Variations in the total abundance of  $C_{37:3-2}$  alkenones represent changes in coccolithophore productivity, one of the most important marine primary producers (Volkman et al., 1980).

## 2. Materials and Methods

### 2.1. Site U1475

Sediment samples from Site U1475 were collected during the International Ocean Discovery Program (IODP) Expedition 361 in 2016. IODP Site U1475 (41°25.61'S; 25°15.64'E, 2,669 mbsl) is located south of Africa on the southwestern flank of the Agulhas Plateau (Figure 1) (Hall, Hemming, LeVay, Barker, Berke, Brentegani et al., 2017). Site U1475 offers a strategic location to study latitudinal migrations of the STF; it currently lies between the far northern edge of the modern STF and the ARC path (Hall, Hemming, LeVay, Barker, Berke, Brentegani et al., 2017; Hall, Hemming, LeVay, Barker, Berke, Caley et al., 2017). Sediments recovered using an advanced piston coring system from Holes U1475B, U1475C, U1475E, and U1475F were spliced together to generate a continuous sequence (~292 m CCSF) based on RGB blue, b\* color reflectance, and natural gamma radiation (NGR) data (Hall, Hemming, LeVay, Barker, Berke, Brentegani et al., 2017; Hall, Hemming, LeVay, Barker, Berke, Caley et al., 2017). In total 352 samples were selected from the interval of the splice spanning from 1.4–0.3 Ma to generate organic geochemistry records at the Agulhas Plateau with an average resolution of approximately 3 kyr. The Site U1475 age model (Starr et al., 2021) is based on the correlation of the benthic foraminifera *Cibicides wuellerstorfi* stable oxygen isotope ( $\delta^{18}\text{O}$ ) record from sediments recovered from Site U1475 to the global  $\delta^{18}\text{O}$  stack (Ahn et al., 2017; Lorraine E. Lisiecki & Raymo, 2005).

### 2.2. Biomarker Analyses

Sediment samples collected every 6–8 cm were freeze-dried and homogenized. To obtain the total lipid extract (TLE), lipids were extracted using an Accelerated Solvent Extractor (Dionex ASE 350) using a mixture of 9:1 (v:v) dichloromethane (DCM): methanol (MeOH). An aliquot of the TLE was dried with a gentle stream of ultrapure  $\text{N}_2$  gas for chlorin concentrations. The chlorin aliquot was then re-dissolved using acetone and transferred to a quartz cuvette where it was analyzed using a UV/Vis spectrophotometer (Thermo Scientific Genesys 10 UV). Readings were taken in triplicate at both 410 and 665 nm wavelength, the absorption maximum of chlorophyll-derived chlorin pigments (Rosell-Melé et al., 1997), to calculate mean chlorin concentration per sample.

To obtain the apolar, neutral, and polar fractions from the TLE, each sample was passed through an alumina oxide ( $\text{Al}_2\text{O}_3$ ) column chromatography, using hexane/DCM 9:1, hexane/DCM 1:1, and DCM/MeOH 1:1 as eluents, respectively. The neutral fractions, containing  $\text{C}_{37:3-2}$  alkenones, were identified and quantified using a Thermo Scientific Trace 1310 GC-FID coupled to an ISQ MS system using  $5\alpha$ -Androstane as an internal standard. The Trace 1310 GC was equipped with an Rtx-5 column (60 m  $\times$  0.25 mm  $\times$  0.25  $\mu\text{m}$ ) with a temperature program started at 70°C, then increased by 20°C/min to 130°C, and finally, increasing by 4°C/min up to 320°C, where it was held for 20 min. Reproducibility based on replicated analysis of selected samples was  $\pm 0.02 U_{37}^{\text{K}}$  units, which is equivalent to approximately 0.5°C.

Chlorin and alkenone abundances were converted to mass accumulation rates (MARs) using linear sedimentation rates and dry bulk density estimates (Starr et al., 2021).

Two proxies were used to estimate temperature values through time near the water-air surface. One is based on the ratio between the di- and tri-unsaturated alkenones, known as the  $U_{37}^{\text{K}}$  ratio (Brassell et al., 1986; Prahl & Wakeham, 1987). The  $U_{37}^{\text{K}}$  index was calculated using Equation 1, as described by Prahl and Wakeham (1987):

$$U_{37}^{\text{K}} = \frac{C_{37:2}}{C_{37:2} + C_{37:3}} \quad (1)$$

Using this index, SSTs were calculated using Equation 2 which is based on the core top calibration of Müller et al. (1998), and covers a temperature range of 0°C–27°C with a calibration error of  $\pm 1.5^\circ\text{C}$ .

$$U_{37}^{\text{K}} = 0.033(\text{SST}) + 0.044 \quad (2)$$

The second proxy used to track changes in upper water column temperatures is TEX<sub>86</sub> index (Schouten et al., 2002). Polar fractions were filtered (0.45 μm PTFE filter), dried under N<sub>2</sub>, and then dissolved in 99:1 hexane: isopropanol for analysis. GDGTs were analyzed using an Agilent 1260 series high-performance liquid chromatography (HPLC) coupled to an Agilent 6120 single quadrupole mass detector. The instrument was set up according to Hopmans et al. (2015), using two UHPLC silica columns in series at 30°C, to ensure separation of the GDGT compounds. The flow rate was set at 0.2 mL/min. Using hexane as solvent A and hexane: isopropanol (9 : 1, v: v) as solvent B, GDGTs were eluted for 25 min with 82%A and 18%B, then to 62% A and 35% B for 25 min, and finally, 0%A and 100%B for 30 min. GDGTs were quantified using single ion monitoring (SIM) mode of the M + H<sup>+</sup> ions.

The TEX<sub>86</sub> index was calculated using Equation 3 as described by Schouten et al. (2002):

$$\text{TEX}_{86} = \frac{([\text{GDGT} - 2] + [\text{GDGT} - 3] + [\text{Cren}'])}{([\text{GDGT} - 1] + [\text{GDGT} - 2] + [\text{GDGT} - 3] + [\text{Cren}'])} \quad (3)$$

TEX<sub>86</sub> values were converted to SSTs using the BAYSPAR Bayesian spatially varying regression (Tierney & Tingley, 2014, 2015). A comparison to TEX<sub>86</sub>-derived temperatures obtained using other global core-top calibrations (Kim et al., 2008, 2010) can be found in Figure S1.

To assess the relative amount of soil organic matter input possibly affecting the TEX<sub>86</sub>-derived temperature estimates, the Branched and Isoprenoid Tetraether (BIT) index was calculated using Equation 4 as defined by (Hopmans et al., 2004):

$$\text{BIT} = \frac{([\text{GDGT I}] + [\text{GDGT II}] + [\text{GDGT III}])}{([\text{GDGT I}] + [\text{GDGT II}] + [\text{GDGT III}] + [\text{Cren}])} \quad (4)$$

Variability in the amount of allochthonous terrigenous material reaching the study site was reconstructed based on the abundances of long-chain *n*-alkanes (C<sub>29</sub>-C<sub>33</sub>), which are thought to be synthesized by higher land plants (G. Eglinton & Hamilton, 1967; Ficken et al., 2000). Long-chain *n*-alkanes can reach remote oceanic locations by wind (Bendle et al., 2007; Kawamura, 1995; Simoneit, 1977). The apolar fractions containing long-chain *n*-alkanes were analyzed using a Thermo Scientific Trace 1310 GC-FID coupled to an ISQ MS system. The Trace 1310 GC was equipped with an Rtx-5 column (60 m × 0.25 mm × 0.25 μm) with a temperature program started at 80°C, where it was held for one minute, and then, oven temperature was increased by 13°C/min to 320°C, where it was held for 20 min. *n*-Alkanes were identified using the ISQ MS system and by comparison with an external C<sub>7</sub>-C<sub>40</sub> *n*-alkane standard mixture, and finally, quantified using 1,1'-binaphthyl as an internal standard.

### 2.3. Wavelet Analysis

Periodic variability within the records from Site U1475 was analyzed using a continuous wavelet transform method (Grinsted et al., 2004). Alkenone-derived SST and primary productivity records were linearly interpolated to a uniform spacing of 3 kyr. The chlorin-derived primary productivity and the TEX<sub>86</sub>-derived temperature records were linearly interpolated to a uniform spacing of 4 and 5 kyr resolution, respectively.

## 3. Results

### 3.1. Temperature Reconstructions

The two proxy temperature records (Figure 2a) are significantly correlated ( $R = 0.6$ ) and yield similar mean values across the entire record (18.9°C for U<sub>37</sub><sup>K'</sup> and 18.8°C for TEX<sub>86</sub>). The U<sub>37</sub><sup>K'</sup> record ( $n = 339$ ) exhibits a long-term cooling (~2°C) and temperatures range between 15.7°C and 22.8°C. However, the TEX<sub>86</sub>-based record ( $n = 216$ ) shows almost no cooling trend across the entire record, with temperatures ranging between 13.2°C and 25.6°C. The BIT index always exhibits values lower than 0.1 (Figure 2c).

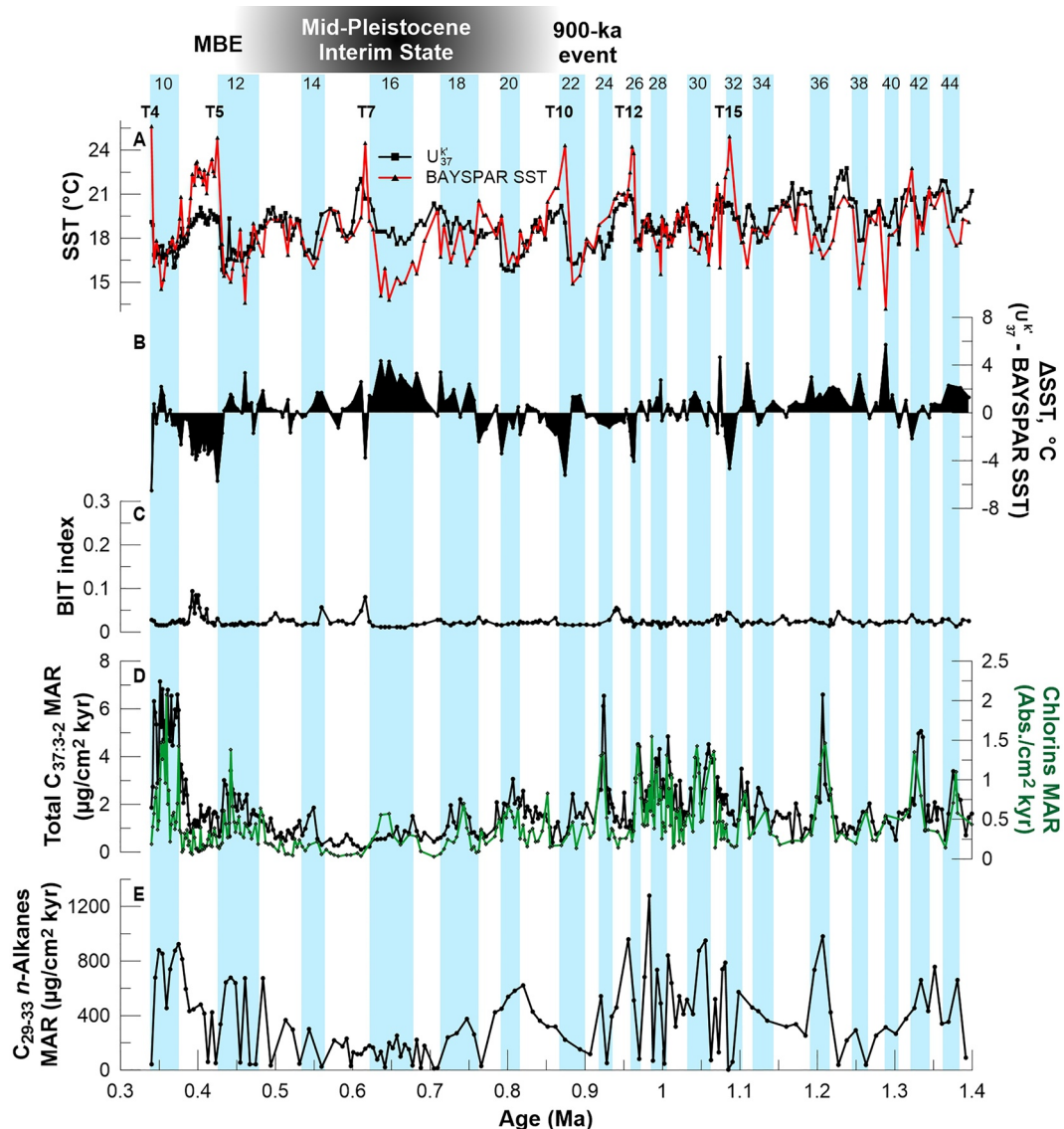


**Figure 2.** Upper water column temperature and productivity records at Site U1475 across the mid-Pleistocene Tetraether. (a) Alkenone- (black) and  $\text{TEX}_{86}$ -derived (red) temperature estimates; (b) temperature offset between the alkenone- and  $\text{TEX}_{86}$ -derived temperature estimates; (c) branched and isoprenoid Tetraether index; (d) productivity records from alkenones (black line) and chlorins (green line) mass accumulation rates (MARs); (e) long-chain n-alkane ( $\text{C}_{29-33}$ ) MARs. Glacial periods are highlighted, and *T* indicates glacial terminations. Numbers at the top of the figure refer to marine isotopic stages.

Prior to the onset of the MPT, ca. 1.2 Ma,  $\text{TEX}_{86}$ -derived temperature estimates are generally similar to or lower than  $U_{37}^K$  temperatures (Figure 2b). The  $U_{37}^K$  record shows a cooling trend prior to the MPT, while the  $\text{TEX}_{86}$ -derived record is somewhat stable. After 0.9 Ma, some interglacial periods show warmer  $\text{TEX}_{86}$ -derived estimates than those from  $U_{37}^K$ , such as during MIS 25, 21, 19, 15, 11, and 9. During 0.8–0.47 Ma, the MPIS, temperatures are relatively stable, however, the  $U_{37}^K$ -derived temperature estimates exhibit lower amplitude glacial-interglacial variability compared to the periods before and after the MPIS. Additionally, a  $\sim 4^\circ\text{C}$  offset between the two temperature records occurs during MIS 16, where  $\text{TEX}_{86}$  temperatures are lower than  $U_{37}^K$  temperatures. Lastly, during the post-MBE period, from 0.47 to 0.3 Ma, there is an increase in the amplitude of  $\text{TEX}_{86}$ -derived temperature record with an overall warming trend apparent in both records.

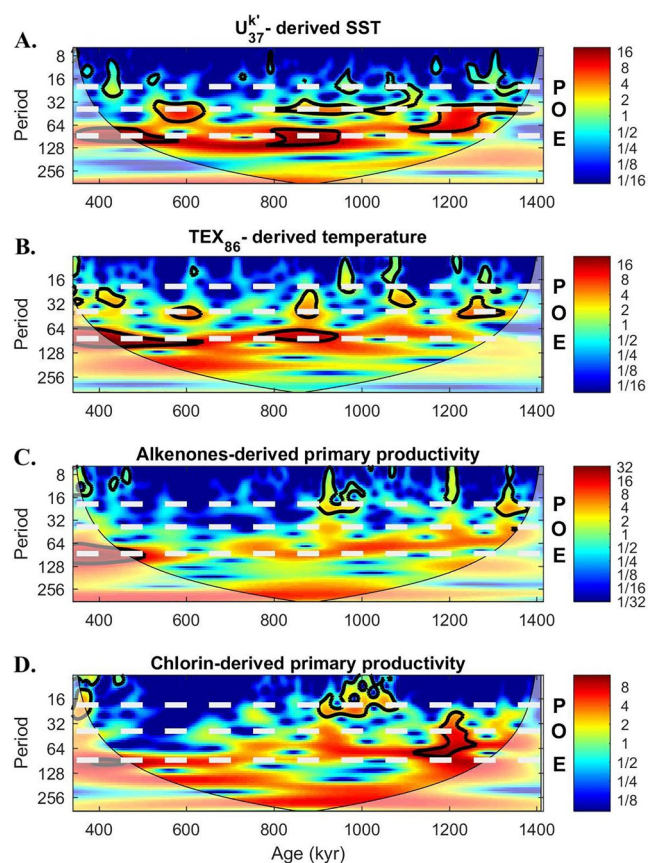


**Figure 3.** Wavelet power spectra for the (a)  $U_{37}^{K'}$ -derived SST; (b)  $TEX_{86}$ -derived temperatures; and (c) alkenone- and (d) chlorin-derived primary productivity records over the mid-Pleistocene transition. Variability at the precession (P), obliquity (O), and eccentricity (E) periods are highlighted. The 5% significance level against red noise is shown as a thick black contour. Spectral density scale on the right side.

### 3.2. Sea Surface Productivity Records

The alkenone-based ( $n = 352$ ) and chlorin-based ( $n = 276$ ) productivity records show a positive, strong correlation ( $R = 0.6$ ) and higher overall productivity during glacial periods relative to interglacials (Figure 2d). MIS 36, 24, and 10 are the glacial intervals with the highest primary production throughout both records. The productivity records show disparities at MIS 14 and the second half of MIS 16. The second half of MIS 16 exhibits the opposite behavior of MIS 14, in this case where the chlorin concentration remains high while the total concentration of  $C_{37:3-2}$  is significantly lower.

### 3.3. *n*-Alkanes

Long-chain *n*-alkanes indicative of allochthonous terrigenous material potentially derived from higher plants were detected in the 133 samples that were selected for this analysis. The total  $C_{29}$ – $C_{33}$  MARs varied between 4.5 and 1,279.7  $\mu\text{g}/\text{cm}^2$  kyr (Figure 2e). *n*-Alkanes exhibit carbon preference indices (CPI<sub>25–35</sub>) between 2.3 and 9.4. Abundances of  $C_{29}$ – $C_{33}$  *n*-alkanes generally show higher MARs during glacial periods than interglacials (Figure 2e).

### 3.4. Wavelet Analysis

Wavelet analyses of the  $U_{37}^{K'}$ ,  $TEX_{86}$  derived upper water temperatures, and total  $C_{37:3-2}$  alkenones MAR (Figures 3a–3c) reveal strong obliquity cycles only prior to 1.1 Ma. After  $\sim 1.0$  Ma, wavelet analyses show established strong 100 kyr eccentricity cycles. Although the shift from 41- to 100-kyr periodicities based on the chlorin-derived primary productivity record (Figure 3d) is not as abrupt as in the other three records, the onset of dominant 100 kyr cycles is seen beginning  $\sim 1.1$  Ma, becoming clear  $\sim 0.8$  Ma.

## 4. Discussion

### 4.1. Comparison of $TEX_{86}$ and $U_{37}^{K'}$ Temperature Records

Our temperature records exhibit an in-phase, glacial-interglacial variability (Figure 2a), but often display an offset from each other, most obvious during glacial terminations, strong interglacial periods (MIS 31, 25, 21, 13, 11, and 9), and MIS 16. These offsets, as large as  $\sim 4^\circ\text{C}$ , are unlikely to be due to calibration uncertainties (Müller et al., 1998; Tierney & Tingley, 2014), and instead, they appear to respond consistently to glacial-interglacial variability and changes in the oceanographic regime (Figure 2a). Diagenetic alteration or soil contamination of the signal do not offer satisfying explanations either. Sedimentary diagenesis does not have a significant effect on  $TEX_{86}$  (Huguet et al., 2006; Kim et al., 2009; Schouten et al., 2004). Alkenones can be affected by oxic degradation (Herbert, 2003), but an oxic experiment showed that the  $U_{37}^{K'}$  index exhibits only a small increase with degradation (0.03 units, equivalent to  $<1^\circ\text{C}$ ) (Tece et al., 1998). BIT values are lower than 0.1 throughout the record, indicating low contributions of soil-derived brGDGTs at Site U1475 (Figure 2c).

Another possible explanation of temperature and productivity trends seen at Site U1475 includes lateral transport of the fine fraction of sediments, including biomarkers (Ohkouchi et al., 2002). Although we cannot completely rule out a non-local source of biomarkers due to lateral transport, we do not think there is substantial offset in our records.  $TEX_{86}$  has been previously shown to be more representative of a local signal, due to more rapid sink of GDGTs from aggregation and opal packaging (Schouten et al., 2013; Wuchter et al., 2005) than alkenones (Mollenhauer et al., 2005, 2007; Shah et al., 2008). The strong coherence in

variability throughout the temperature records at U1475 does not support post-deposition degradation or lateral transport, which would likely have a more independent effect on these proxies. The correspondence between temperature records arguing for minimal transport explanation is similar to observations of biomarker temperature records offshore Australia for the last 135 ka (Lopes dos Santos et al., 2013) and  $U_{37}^K$ -derived SST and foraminiferal assemblage temperature estimates offshore New Zealand for the last 60 ka (Sikes et al., 2002).

Alternatively, the offsets between  $TEX_{86}$ - and  $U_{37}^K$ -derived estimated temperatures could be related to non-thermal factors affecting the  $TEX_{86}$ -derived temperature estimates. GDGT indices to examine the influence of non-thermal factors on the  $TEX_{86}$ -derived temperature estimates suggest little influence by methanogenic archaea or water column migration of archaeal populations (Figure S2).

We also considered whether differences between the two temperature estimates could result from seasonal timing of haptophyte algae and Thaumarchaeota production (Auderset et al., 2019; Castañeda et al., 2010; Huguet et al., 2007). Present-day SSTs at Site U1475 show seasonal variability, and range between 17°C during the summer and 14°C during the winter (Schlitzer, 2014). In several glacial terminations preceding strong interglacials (Terminations 15, 12, 10, 7, 5, and 4) and MIS 11 (Figure 2a), known as a “super-interglacial” (Melles et al., 2012),  $TEX_{86}$  temperatures are considerably higher than  $U_{37}^K$  estimates. This suggests that abrupt and intense warming events may promote seasonal differences between the timing of haptophyte and Thaumarchaeota blooms at the Agulhas Plateau, as has been proposed in other locations (Auderset et al., 2019; Castañeda et al., 2010; Huguet et al., 2007). Furthermore, it has been shown that the seasonal timing of haptophyte algae and Thaumarchaeota blooms may differ (Murray et al., 1999; Wuchter et al., 2005). Thus, at the Agulhas Plateau it could be possible that during glacial terminations that precede strong interglacials, Thaumarchaeota blooms occur during the summer while haptophyte blooms occur during a colder season. However, modern satellite observations indicate that primary productivity in the south of Africa consists of intermittent blooms that mainly take place during the austral spring-summer (Llido et al., 2005), and there is currently no additional data on bloom timing of Thaumarchaeota or haptophyte algae in the area. In summary, while we cannot entirely rule out seasonal timing of blooms contributing to temperature offsets, we do not view this as the most likely explanation for temperature differences observed across these records.

The most probable explanation for the offset between the two temperature records is that  $U_{37}^K$ -derived temperatures reflect surface temperatures while  $TEX_{86}$ -derived estimates reflect values of shallow subsurface temperatures. GDGTs are thought to be produced by chemoautotrophic nitrifiers (Brochier-Armanet et al., 2008) that can live within subsurface water masses (~50–200 m) (Karner et al., 2001; Könneke et al., 2005), in some cases, close to the thermocline (Huguet et al., 2007). Alkenones are synthesized by haptophyte algae and must live within the photic zone (Brassell et al., 1986; Müller et al., 1998) while Thaumarchaeota tend to grow in the upper oxic to anoxic chemocline (Becker et al., 2018; Lam et al., 2007; Stahl & de la Torre, 2012; Stewart et al., 2012; Wakeham et al., 2007). Indeed, over the last 3.5 Ma, significant offsets between  $TEX_{86}$ - and  $U_{37}^K$ -derived temperature records have been shown in the southeast Atlantic Ocean (Site 1087) within the Benguela Upwelling System (Petrick et al., 2018). Intervals where  $TEX_{86}$ -derived temperatures show a significant offset to  $U_{37}^K$ -derived estimates could be explained by shallower mixed layer depths and well stratified waters, which would be indicative of Subtropical AC waters over Site U1475. Stratified waters may cause warm rather than cold bias in the reconstructed  $TEX_{86}$ -derived temperatures because strong stratification may drive oxygen minimum zones toward the photic zone. It has been shown that increases in oxygen limitation led to higher  $TEX_{86}$  values (Qin et al., 2015). Thus, well stratified waters could also explain warmer  $TEX_{86}$ - than  $U_{37}^K$ -derived temperatures. Intervals where  $U_{37}^K$ - and  $TEX_{86}$ -derived temperatures are similar could be explained by a deeper mixed layer depth and well-mixed upper water column, as seen in Subantarctic waters.

#### 4.2. Latitudinal Migrations of the Subtropical Front

The STF is the hydrographic boundary that marks the northern extent of Subantarctic waters (Orsi et al., 1995). Currently, the highest chlorophyll-*a* concentration in the Southern Ocean is found between the

STF and SAF (Read et al., 2000). Thus, changes in both primary productivity and upper ocean temperatures at sites such as Site U1475 located north of the present-day STF position can be used to indicate potential meridional expansions of the Southern Ocean and associated frontal shifts through time.

Although biomarker preservation may affect estimates of productivity, we consider and compare both chlorins and alkenones, independently analyzed and measured, and produced by different groups. In the absence of any geochemical evidence to suggest degradation or preservation differences, we note similar trends shown by alkenones and chlorins, suggesting both are similarly associated with changes in primary productivity at the Agulhas Plateau. Additionally, glacial-interglacial productivity differences presented here have also been documented from sites in the Southwest Indian Ocean (Bard & Rickaby, 2009; Martínez-García et al., 2009; Romero et al., 2015) and Southeast Atlantic (Petrick et al., 2018; Rosell-Melé et al., 2014), suggesting these trends in productivity are not unexpected.

Changes in upper water column stratification may also reflect expansions of the Southern Ocean. Shallower mixed layer depths distinguish Subtropical from Subantarctic waters in all seasons at  $\sim 25^\circ\text{E}$  (Holte & Talley, 2009) (Figure 1b). Throughout the last 1.4 Ma, chlorin and alkenone productivity increases during glacial intervals, consistent with the late Quaternary data (Romero et al., 2015), suggesting an expansion of the nutrient-rich waters of the Southern Ocean northwards. Convergence in surface and subsurface temperatures indicate a less stratified upper column during many glacials (Figure 2b) while warm intervals often show more stratified upper column waters (Figure 2b) (Flores et al., 1999) and shallow mixed layer depths (Holte & Talley, 2009) indicative of AC waters over the site. Below we discuss the expansion and contraction of the Southern Ocean.

#### 4.2.1. 1.4 to 1.1 Ma (MIS 45-34)

From 1.4 to 1.1 Ma, when  $U_{37}^K$ -derived SSTs are consistently higher than  $TEX_{86}$ -derived water temperatures ( $\sim 2^\circ\text{C}$  on average) at the Agulhas Plateau (Figure 2a), the uppermost water column is inferred to have been somewhat stratified, likely influenced by the ARC, while the STF was in a more southerly position. Due to stratified nature of the upper water column and lack of nearby nutrient-rich Southern Ocean waters at Site U1475 (Lutjeharms, 2006; Orsi et al., 1995; Read et al., 2000), we attribute productivity increases during MIS 44, 42, and 36 to the relatively significant amounts of wind-blown terrestrial material, evidenced by increases in long-chain *n*-alkanes ( $C_{29}$ - $C_{33}$ ) (Figure 2e). Increases of wind-blown terrestrial organic material in remote areas have been previously used to identify dust deposition at Site 1090 (Martínez-García et al., 2011), with dust supplying essential limiting micronutrients such as iron (Simoneit, 1977) in times with little to no mixing. Glacial increases of dust deposition in the Southern Ocean have been proposed to stimulate primary productivity at nearby Site 1090 (Martínez-García et al., 2011). MIS 36 ( $\sim 1.2$  Ma) coincides with the development of the first Northern Hemisphere continental-scale ice sheets (Mudelsee & Statterger, 1997) and strengthening of glacial-interglacial circulation contrasts in the Atlantic Ocean circulation after 1.2 Ma (Diekmann & Kuhn, 2002). Thus, the increases in productivity exhibited during MIS 44, 42, and 36 (Figure 2d) could be in response to the pulses of wind-blown material deposited in the area (Figure 2e).

#### 4.2.2. 1.1 to 0.9 Ma (MIS 33-24)

Between 1.1 and 0.9 Ma  $TEX_{86}$  and  $U_{37}^K$  temperatures are somewhat lower than found in MIS 45-34, but similar to one another. An exception to the similarity is found at the glacial terminations that preceded strong interglacials (MIS 31 and MIS 25). Productivity was elevated and highly variable between MIS 31-24 (Figures 2d and S3), suggesting increased nutrient supply from the Southern Ocean. This is consistent with a northward migration of the STF, placing the front near the Agulhas Plateau during this interval.

The glacial termination preceding MIS 31 (T15) and MIS 25 (T12) have  $TEX_{86}$ -derived temperatures that are significantly higher than  $U_{37}^K$ -derived SSTs (Figure 2a). These warming events correlate with decreased productivity (Figure 2d) and may have been the result of abrupt southward retreats of the STF. MIS 31 has been widely investigated as an extremely warm period in both hemispheres (Froelich et al., 1991; Lisiecki & Raymo, 2005; Marino et al., 2009; Melles et al., 2012; Pollard & DeConto, 2009; Teitler et al., 2015), and may represent a precursor of the high-amplitude 100-kyr climate cycles of the Late Pleistocene (Scherer et al., 2008). The extreme warming observed during MIS 31 has been linked to a possible collapse of the West Antarctic Ice Sheet in response to a 2-5°C increase in SSTs of the Antarctic oceans (Pollard &

DeConto, 2009), and a southward shift of the STF (Maiorano et al., 2009) and APF (Flores & Sierro, 2007; Froelich et al., 1991) in the South Atlantic sector. Analyses of calcareous nannofossil abundances and mineralogical proxies at ODP Site 1090 suggest that the major climate modification experienced during MIS 31 led not only to a poleward shift of the STF, but also to an expansion of the influence of the warmer AC in the eastern subantarctic sector of the South Atlantic Ocean (Maiorano et al., 2009). Thus, temperatures during T15 and T12 (Figure 2) might indicate a higher sensitivity of GDGT producers to a shallower mixed layer depth caused by a drastic retreat of the STF and a strong presence of AC waters over the Agulhas Plateau.

#### 4.2.3. 0.9 to 0.47 Ma (MIS 23-13)

The onset of the dominant 100-kyr cycles (Figure 3) in the MPIS coincides with increases in the offset between the two temperature records and progressively lower productivity in successive glacial records (Figures 2a and 2d). These signals are consistent with subtropical-like conditions over the southern Agulhas Plateau and a more southerly position of the STF and the subantarctic, nutrient-rich waters, relative to Site U1475. Taken together, our records indicate that during the MPIS, upper water temperatures and productivity suggest a strong influence of the ARC at Site U1475 consistent with a southward retreat of the STF south of Africa and long-term contraction of the Southern Ocean. Moreover, our records also show modest glacial-interglacial variability, which suggests that latitudinal migrations of the STF still took place over glacial-interglacial periods. However, those migrations were minor in comparison to higher amplitude variability observed before and after the MPIS.

#### 4.2.4. 0.47 to 0.3 Ma (MIS 12-9)

The MBE (~0.42 Ma) marks the end of the interval where the STF generally remained in a more southerly position. We see abrupt glacial-interglacial temperature and primary productivity variability after the MBE. Between MIS 12–9, we observe low primary productivity and  $TEX_{86}$ -derived temperatures lower than  $U_{37}^K$ -derived SST during interglacial periods, while there are similar  $TEX_{86}$ - and  $U_{37}^K$ -derived temperature estimates and increasing primary productivity during glacial periods (Figure 2). After the MBE, very different glacial-interglacial oceanographic conditions are seen at the Agulhas Plateau. Warmer subsurface waters ( $TEX_{86}$ -derived) than SSTs ( $U_{37}^K$  estimates) and the lowest productivity of the entire record occur during MIS 11 (Melles et al., 2012), the warmest and longest interglacial of the last 5 million years (Lisiecki & Raymo, 2005). These results suggest that during MIS 11, the uppermost waters overlying the Agulhas Plateau were mostly subtropical and the STF abruptly migrated to a more southward position relative to the Agulhas Plateau. MIS 10 displays similar  $TEX_{86}$ - and  $U_{37}^K$ -derived temperatures and an increase in primary productivity at Site U1475, suggesting a northward migration of STF closer to the Agulhas Plateau. During MIS nine upper water temperatures and productivity at Site U1475 are similar to the ones during MIS 11, which suggests poleward migration of the STF. Together, these records suggest that following the MBE, more exaggerated glacial-interglacial latitudinal migrations of the STF occurred at the Agulhas Plateau.

### 4.3. Implications for Ocean Circulation and Global Climate

Latitudinal migrations of the STF have been suggested to play a role in modulating Agulhas Leakage, thus impacting the AMOC and global climate. Shifts of the meridional position of the STF over glacial-interglacial and longer timescales from 1.4 to 0.3 Ma are suggested with our multiproxy reconstructions of upper water temperatures and productivity. However, other factors such as modulation of Agulhas Leakage, ocean circulation changes, and  $CO_2$  variability may also be at play.

To examine these other likely linkages, we compare our results to records of accumulation rates of *Globobulimina menardii* at Site 1087 (Figure 4c), interpreted as an indicator of Agulhas Leakage (Caley et al., 2012). Although Sexton and Norris (2011) suggest that *G. menardii* variability track poorly ventilated thermocline waters, Caley et al. (2012) demonstrated that the presence and absence of *G. menardii* at Site 1087 compares well with the Agulhas Leakage fauna record (Peeters et al., 2004), reconstructed based on planktic foraminifera abundance over the last 560 kyr. Studies have shown that Agulhas Leakage fauna generally increases (decreases) during interglacial (glacial) periods due to an enhanced (reduced) Agulhas Leakage (Caley et al., 2012; Peeters et al., 2004). The comparison between our interpreted changes in the position of the STF and the *G. menardii*-derived Agulhas Leakage variability show that only the most significant

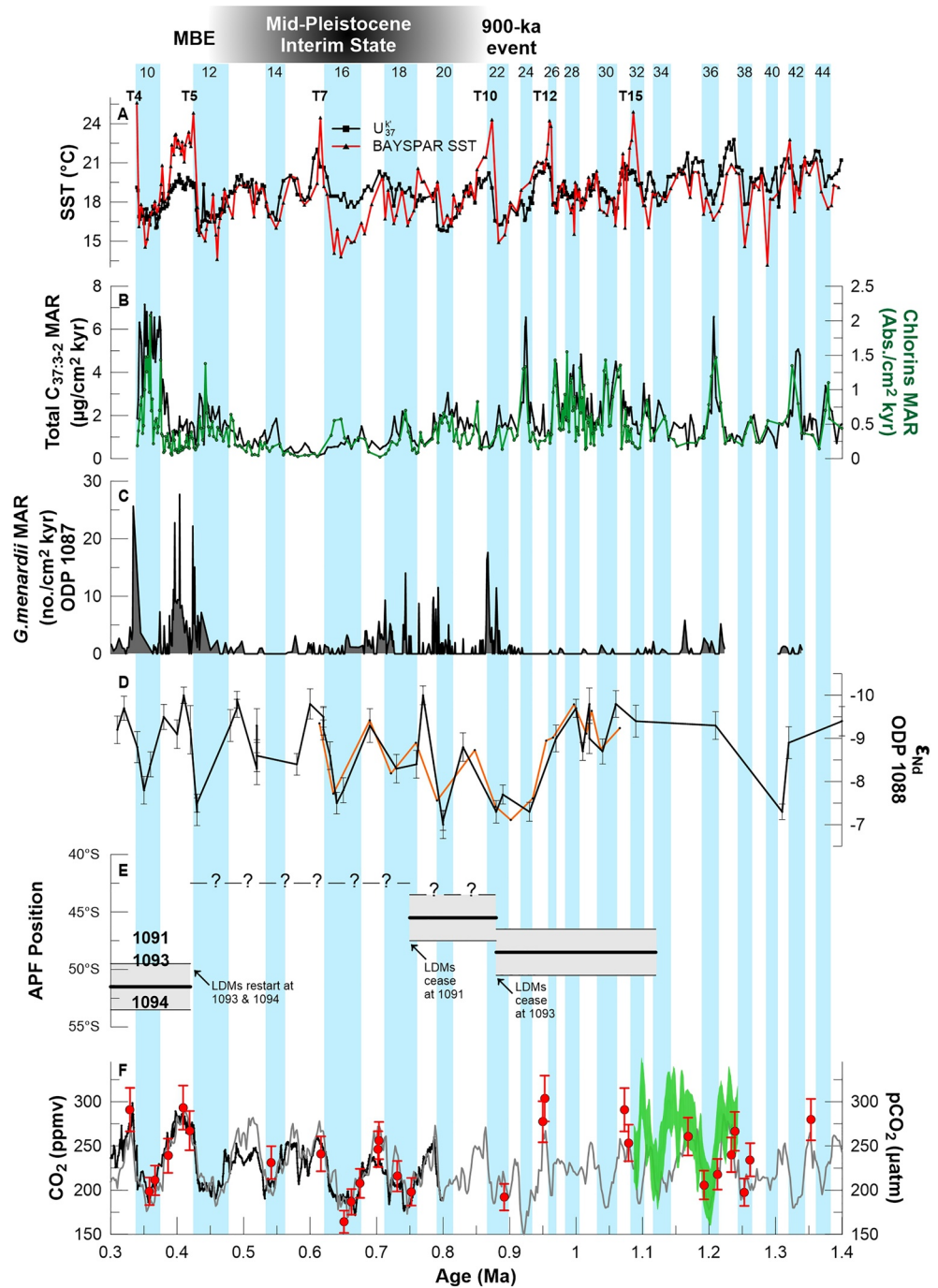


**Figure 4.** Upper water column variability at and near the Agulhas Plateau. (a) Alkenone-derived (black) and TEX<sub>86</sub>-derived (red) temperature estimates at Site U1475; (b) productivity records using alkenones (black line) and chlorins (green line) abundances at Site U1475; (c) Agulhas Leakage based on accumulation rates of *G. menardii* at Site 1,087 (Caley et al., 2012); (d) variability of neodymium isotope ratios ( $\epsilon\text{Nd}$ ) at Site 1088 representing changes in Atlantic meridional overturning circulation strength (Dausmann et al., 2017; Peña & Goldstein, 2014); (e) schematic of latitudinal migrations of the Antarctic Polar Front based on the laminated diatom mats occurrence at Sites 1091, 1093, and 1094 (Kemp et al., 2010); (f) atmospheric CO<sub>2</sub> concentration from the EPICA ice core (black line) (Lüthi et al., 2008; Pépin et al., 2001; Petit et al., 1999; Raynaud et al., 2005), from  $\delta^{13}\text{C}$  models (gray line) (Lisiecki, 2010), and from planktic foraminiferal boron isotopes (red circles) (Hönisch et al., 2009) and (green curve) (Chalk et al., 2017). Glacial periods are highlighted, and T indicates glacial terminations. Numbers at the top of the figure refer to marine isotopic stages.

northward migrations of the STF (MIS 34–24 and MIS 10) coincide with an interruption of Agulhas Leakage (Figure 4). During periods where the STF is located in its most southerly position or glacial periods with less northward migration of the STF, the *G. menardii*-derived Agulhas Leakage does not seem to respond to changes in the STF position. Thus, it appears that the latitudinal position of the STF only regulates Agulhas Leakage when the STF reaches a significantly northward location. Some other dynamical mechanism must control Agulhas Leakage during periods where the STF has not significantly moved northward but leakage fauna decreased.

We also compare with lower-resolution records of neodymium isotope ratios ( $\epsilon_{Nd}$ ) at Site 1088 (Figure 4d) (Dausmann et al., 2017; Peña & Goldstein, 2014) to examine whether latitudinal migrations of the STF relate to deep ocean circulation fluctuations. Comparison between  $\epsilon_{Nd}$  values of intermediate waters from the nearby Agulhas Ridge and our hypothesized Agulhas Plateau STF migrations also suggest that changes in the AMOC variability are not always directly related to the overall position of the STF. For example, the expansion of the Southern Ocean at MIS 34–24 and MIS 10 show an interruption in leakage, but high  $\epsilon_{Nd}$  values do not suggest an AMOC slow down during those periods (Figure 4), at the resolution available. Additionally, a significant reduction in North Atlantic-sourced water masses is seen prior to the 900-kyr event (Figure 4d; Dausmann et al., 2017; Peña & Goldstein, 2014), which coincides with the beginning of the southward retreat of the STF. As the STF continues toward a more southerly position during the MPIS, the  $\epsilon_{Nd}$  records begin to show glacial-interglacial AMOC variability that does not resemble the modest glacial-interglacial migrations of the STF during that interval.

Comparing our temperature and productivity results from the Agulhas Plateau with AMOC and Agulhas Leakage variability suggests that there is a disconnect between STF migrations and leakage volume during intervals within the MPIS. This possible decoupling has been previously linked to variability in the intensity of the Southern Hemisphere westerlies helping modulate throughflow between the western Indian and south Atlantic Oceans (De Boer et al., 2013; Durgadoo et al., 2013; Graham & Boer, 2013). Using modeling experiments, Durgadoo et al. (2013) showed Agulhas Leakage responded to westerly wind strength, with shifts north (south) in the westerlies enhancing (diminishing) leakage. Displacement of the wind belt momentum, potentially due to the physical presence of the plateau, is thought to be responsible for the change in leakage volume, with the resulting redistribution of this energy (Durgadoo et al., 2013) counter to the STF explanation of leakage control of Bard and Rickaby (2009). Thus, changes in leakage volume or AMOC variability that do not appear to be correlated to STF migrations as determined by our temperature and productivity reconstructions, such as the major stagnation of the AMOC following the 900-kyr event (Figure 4d, Dausmann et al., 2017; Peña & Goldstein, 2014), may be connected instead to shifts in westerly winds, as previously modeled.

We see lower amplitude changes in temperature and productivity and lower Southern Ocean influence at Site U1475 when global atmospheric CO<sub>2</sub> variations are relatively muted during the MPIS. Intervals with northward shifts in the westerlies, previously described as linked to enhanced Agulhas Leakage (Durgadoo et al., 2013), are also thought to allow the accumulation of CO<sub>2</sub> within the deep ocean (Toggweiler et al., 2006). Movement of the westerlies away from the Southern Ocean are thought to reduce CO<sub>2</sub> ventilation from deep waters (Toggweiler et al., 2006), thus connecting hypothesized northward westerly wind shifts with evidence of relatively low atmospheric CO<sub>2</sub> values during the MPIS (Hönisch et al., 2009; Lüthi et al., 2008) (Figure 4f).

Although an expansion of the Southern Ocean during the MPIS has been previously suggested (Kemp et al., 2010), we do not see temperature or productivity evidence of such an expansion between 0.9 to 0.47 Ma. A northward migration of the APF has been proposed to take place during the MPIS based on the disappearance of laminated diatom mats at Sites 1091, 1093, and 1094 (Kemp et al., 2010) implying an expansion of the Southern Ocean. Moreover, a new record of ice-rafted debris (IRD) from Site (Starr et al., 2021) suggests that the long-term cooling trend during the MPIS may have provided increasingly iceberg-favorable conditions at Site U1475, which had a significant impact on freshwater redistribution in the Southern Ocean across the MPT. Expansions of the Southern Ocean have been proposed to play a role in regulating atmospheric CO<sub>2</sub> (Kemp et al., 2010; Lüthi et al., 2008). While our temperature and productivity records from Site U1475 may not indicate an expansion of the Southern Ocean during the MPIS, our

data may support low atmospheric CO<sub>2</sub> at this time related to reduced deep water ventilation from shifting westerlies (Toggweiler et al., 2006) or diminished drawdown of CO<sub>2</sub> from reduced primary productivity.

## 5. Conclusions

We examine changes in the latitudinal position of the STF over the last 1.4–0.3 Ma based on new records of upper water column temperatures and productivity from IODP Site U1475 on the Agulhas Plateau. Our records show that the latitudinal position of the STF not only exhibits glacial-interglacial variability, but also likely latitudinal migrations over longer timescales. Our results support northward migrations of the STF during glacial and southward migrations during interglacial periods. On longer timescales, our multi-proxy data suggest that the STF reached its northernmost position during MIS 34–24 and MIS 10. Comparisons with *G. menardii* at nearby Site 1087 (Caley et al., 2012) and with records of  $\epsilon_{\text{Nd}}$  at nearby Site 1088 (Dausmann et al., 2017; Peña & Goldstein, 2014) suggest that only these significant northward migrations interrupted Agulhas Leakage and potentially altered the AMOC. During the MPIS, the STF migrated to its most southerly position relative to Site U1475. Based on our data, there is a significant southward migration of the STF during the MPIS that coincides with relatively low atmospheric CO<sub>2</sub> values (Hönisch et al., 2009; Lüthi et al., 2008), enhanced Agulhas Leakage (Caley et al., 2012), and significant glacial increases of IRD reaching the Agulhas Plateau (Starr et al., 2021). Some other dynamical control beyond STF migrations must contribute to Agulhas Leakage and AMOC variability during the MPIS. We suggest that shifts in the Southern Hemisphere westerly winds may account for the circulation changes seen when the STF was in its southernmost position, supporting prior modeling studies that have shown the importance of the westerlies in Agulhas Leakage (Durgadoo et al., 2013). A northward shift in the westerlies might also help explain muted CO<sub>2</sub> levels observed during the MPIS, with reduced deep sea ventilation as winds shift to the north (Toggweiler et al., 2006).

## Data Availability Statement

All data from this study can be found in the World Data Service for Paleoclimatology, run by NOAA (<https://doi.org/10.25921/tjae-sx80>).

## Acknowledgments

We thank the captain and crew of the JOIDES Resolution for their technical support during the recovery of sediment cores used in this study. We thank the International Ocean Discovery Program for the opportunity to sail on Expedition 361 and access Expedition 361 sediment samples. We thank Kristine Mitchell, Dr. Robert Nerenberg, and Dr. Jeff Salacup for assistance in the lab. Funding for this research was made possible through NSF MGG award 1737218 as well as the U.S. Science Support Program Post-Expedition Award, the CEST Bayer Predoctoral Research Fellowship, and the Joseph F. Downes Memorial Award. The authors appreciate the helpful comments and suggestions provided by the anonymous reviewers and editors.

## References

- Ahn, S., Khider, D., Lisiecki, L. E., & Lawrence, C. E. (2017). A probabilistic Pliocene–Pleistocene stack of benthic  $\delta^{18}\text{O}$  using a profile hidden Markov model. *Dynamics and Statistics of the Climate System*, 2(1). <https://doi.org/10.1093/climsys/dzx002>
- Auderset, A., Martínez-García, A., Tiedemann, R., Hasenfratz, A. P., Eglinton, T. I., Schiebel, R., et al. (2019). Gulf Stream intensification after the early Pliocene shoaling of the Central American Seaway. *Earth and Planetary Science Letters*, 520, 268–278. <https://doi.org/10.1016/j.epsl.2019.05.022>
- Bard, E., & Rickaby, R. E. M. (2009). Migration of the subtropical front as a modulator of glacial climate. *Nature*, 460(7253), 380–383. <https://doi.org/10.1038/nature08189>
- Beal, L. M., Chereskin, T. K., Lenn, Y. D., & Elipot, S. (2006). The sources and mixing characteristics of the Agulhas current. *Journal of Physical Oceanography*, 36(11), 2060–2074. <https://doi.org/10.1175/JPO2964.1>
- Beal, L. M., De Ruijter, W. P. M., Biastoch, A., Zahn, R., Zahn, R., & SCOR/WCRP/IAPSO Working Group 136. (2011). On the role of the Agulhas system in ocean circulation and climate. *Nature*, 472(7344), 429–436. <https://doi.org/10.1038/nature09983>
- Becker, K. W., Elling, F. J., Schröder, J. M., Lipp, J. S., Goldhammer, T., Zabel, M., et al. (2018). Isoprenoid quinones resolve the stratification of redox processes in a biogeochemical continuum from the photic zone to deep anoxic sediments of the Black Sea. *Applied and Environmental Microbiology*, 84(10). <https://doi.org/10.1128/AEM.02736-17>
- Becquey, S., & Gersonde, R. (2002). Past hydrographic and climatic changes in the Subantarctic Zone of the South Atlantic – The Pleistocene record from ODP Site 1090. *Palaeoecology, Palaeoclimatology, Palaeoecology*, 182(3–4), 221–239. [https://doi.org/10.1016/S0031-0182\(01\)00497-7](https://doi.org/10.1016/S0031-0182(01)00497-7)
- Belkin, I. M., & Gordon, A. L. (1996). Southern Ocean fronts from the Greenwich meridian to Tasmania. *Journal of Geophysical Research*, 101(C2), 3675–3696. <https://doi.org/10.1029/95JC02750>
- Bendle, J., Kawamura, K., Yamazaki, K., & Niwai, T. (2007). Latitudinal distribution of terrestrial lipid biomarkers and n-alkane compound-specific stable carbon isotope ratios in the atmosphere over the western Pacific and Southern Ocean. *Geochimica et Cosmochimica Acta*, 71(24), 5934–5955. <https://doi.org/10.1016/j.gca.2007.09.029>
- Berger, W. H., & Jansen, E. (1994). Mid-Pleistocene climate shift - The Nansen connection. In M. Johannesen, R. D. Muench, & J. E. Overland (Eds.), *The polar oceans and their role in shaping the global environment. Geophysical monograph series* (pp. 295–311). American Geophysical Union.
- Brassell, S. C., Eglinton, G., Marlowe, I. T., Pflaumann, U., & Sarnthein, M. (1986). Molecular stratigraphy: A new tool for climatic assessment. *Nature*, 320(6058), 129–133. <https://doi.org/10.1038/320129a0>
- Brochier-Armanet, C., Boussau, B., Gribaldo, S., & Forterre, P. (2008). Mesophilic crenarchaeota: Proposal for a third archaeal phylum, the Thaumarchaeota. *Nature Reviews Microbiology*, 6(3), 245–252. <https://doi.org/10.1038/nrmicro1852>

- Caley, T., Giraudeau, J., Malaize, B., Rossignol, L., & Pierre, C. (2012). Agulhas leakage as a key process in the modes of Quaternary climate changes. *Proceedings of the National Academy of Sciences*, 109(18), 6835–6839. <https://doi.org/10.1073/pnas.1115545109>
- Castañeda, I. S., Schefuß, E., Pätzold, J., Sinninghe Damsté, J. S., Weldeab, S., & Schouten, S. (2010). Millennial-scale sea surface temperature changes in the eastern Mediterranean (Nile River Delta region) over the last 27,000 years: Eastern mediterranean SST records. *Paleoceanography*, 25(1), PA1208. <https://doi.org/10.1029/2009PA001740>
- Chalk, T. B., Hain, M. P., Foster, G. L., Rohling, E. J., Sexton, P. F., Badger, M. P. S., et al. (2017). Causes of ice age intensification across the Mid-Pleistocene Transition. *Proceedings of the National Academy of Sciences*, 114(50), 13114–13119. <https://doi.org/10.1073/pnas.1702143114>
- Clark, P. U., Archer, D., Pollard, D., Blum, J. D., Rial, J. A., Brovkin, V., et al. (2006). The middle Pleistocene transition: Characteristics, mechanisms, and implications for long-term changes in atmospheric pCO<sub>2</sub>. *Quaternary Science Reviews*, 25(23–24), 3150–3184. <https://doi.org/10.1016/j.quascirev.2006.07.008>
- Clark, P. U., & Pollard, D. (1998). Origin of the Middle Pleistocene Transition by ice sheet erosion of regolith. *Paleoceanography*, 13(1), 1–9. <https://doi.org/10.1029/97PA02660>
- Dausmann, V., Frank, M., Gutjahr, M., & Rickli, J. (2017). Glacial reduction of AMOC strength and long-term transition in weathering inputs into the Southern Ocean since the mid-Miocene: Evidence from radiogenic Nd and Hf isotopes. *Paleoceanography*, 32(3), 265–283. <https://doi.org/10.1002/2016PA003056>
- De Boer, A. M., Graham, R. M., Thomas, M. D., & Kohfeld, K. E. (2013). The control of the Southern Hemisphere Westerlies on the position of the Subtropical Front. *Journal of Geophysical Research: Oceans*, 118(10), 5669–5675. <https://doi.org/10.1002/jgrc.20407>
- Diekmann, B., & Kuhn, G. (2002). Sedimentary record of the mid-Pleistocene climate transition in the southeastern South Atlantic (ODP Site 1090). *Palaeogeography, Palaeoclimatology, Palaeoecology*, 182(3–4), 241–258. [https://doi.org/10.1016/S0031-0182\(01\)00498-9](https://doi.org/10.1016/S0031-0182(01)00498-9)
- Durgadoo, J. V., Loveday, B. R., Reason, C. J. C., Penven, P., & Biastoch, A. (2013). Agulhas leakage predominantly responds to the Southern Hemisphere Westerlies. *Journal of Physical Oceanography*, 43(10), 2113–2131. <https://doi.org/10.1175/JPO-D-13-047.1>
- Eglinton, G., & Hamilton, R. J. (1967). Leaf Epicuticular Waxes. *Science*, 156(3780), 1322–1335. <https://doi.org/10.1126/science.156.3780.1322>
- Eglinton, T. I., & Eglinton, G. (2008). Molecular proxies for paleoclimatology. *Earth and Planetary Science Letters*, 275(1–2), 1–16. <https://doi.org/10.1016/j.epsl.2008.07.012>
- Elderfield, H., Ferretti, P., Greaves, M., Crowhurst, S., McCave, I. N., Hodell, D., & Piotrowski, A. M. (2012). Evolution of ocean temperature and ice volume through the mid-Pleistocene climate transition. *Science*, 337(6095), 704–709. <https://doi.org/10.1126/science.1221294>
- Ficken, K. J., Li, B., Swain, D. L., & Eglinton, G. (2000). An n-alkane proxy for the sedimentary input of submerged/floating freshwater aquatic macrophytes. *Organic Geochemistry*, 31(7–8), 745–749. [https://doi.org/10.1016/S0146-6380\(00\)00081-4](https://doi.org/10.1016/S0146-6380(00)00081-4)
- Flores, J.-A., Gersonde, R., & Sierro, F. J. (1999). Pleistocene fluctuations in the Agulhas Current Retroflection based on the calcareous plankton record. *Marine Micropaleontology*, 37(1), 1–22. [https://doi.org/10.1016/S0377-8398\(99\)00012-2](https://doi.org/10.1016/S0377-8398(99)00012-2)
- Flores, J.-A., & Sierro, F. J. (2007). Pronounced mid-Pleistocene southward shift of the Polar Front in the Atlantic sector of the Southern Ocean. *Deep Sea Research Part II: Topical Studies in Oceanography*, 54(21–22), 2432–2442. <https://doi.org/10.1016/j.dsr2.2007.07.026>
- Froelich, P. N., Malone, P. N., Hodell, D. A., Ciesielski, P. F., Warnke, D. A., Westall, F., et al. (1991). *Biogenic opal and carbonate accumulation rates in the subantarctic South Atlantic: The Late Neogene of Meteor Rise Site 704*. In P. F. Ciesielski, Y. Kristoffersen, et al. (Eds.), (Vol. 114, pp. 515–550). <https://doi.org/10.2973/odp.proc.sr.114.1991>
- Gordon, A. L. (2003). The branniest retroflection. *Nature*, 421, 904–905. <https://doi.org/10.1038/421904a>
- Graham, R. M., & Boer, A. M. D. (2013). The dynamical subtropical front. *Journal of Geophysical Research: Oceans*, 118(10), 5676–5685. <https://doi.org/10.1002/jgrc.20408>
- Grinsted, A., Moore, J. C., & Jevrejeva, S. (2004). Application of the cross wavelet transform and wavelet coherence to geophysical time series. *Nonlinear Processes in Geophysics*, 11(5/6), 561–566. <https://doi.org/10.5194/npg-11-561-2004>
- Hall, I. R., Hemming, S. R., LeVay, L. J., Barker, S., Berke, M. A., Brentegani, L., et al. (2017). Expedition 361 summary. *Proceedings of the International Ocean Discovery Program*, 361, 33. <https://doi.org/10.14379/iodp.proc.361.104.2017>
- Hall, I. R., Hemming, S. R., LeVay, L. J., Barker, S., Berke, M. A., Caley, T., et al. (2017). Site U1475. *Proceedings of the International Ocean Discovery Program*. <https://doi.org/10.14379/iodp.proc.361.2017>
- Hall, I. R., McCave, I. N., Weedon, G. P., Harris, S. E., & Harris, S. E. (2001). Intensified deep Pacific inflow and ventilation in Pleistocene glacial times. *Nature*, 412, 809–812. <https://doi.org/10.1038/35090552>
- Harris, P. G., Zhao, M., Rosell-Melé, A., Tiedemann, R., Sarntheim, M., & Maxwell, J. R. (1996). Chlorin accumulation rate as a proxy for Quaternary marine primary productivity. *Nature*, 383(6595), 63–65. <https://doi.org/10.1038/383063a0>
- Hayward, B. W., Kawagata, S., Grenfell, H. R., Sabaa, A. T., & O'Neill, T. (2007). Last global extinction in the deep sea during the mid-Pleistocene climate transition. *Paleoceanography*, 22(3), PA3103. <https://doi.org/10.1029/2007PA001424>
- Herbert, T. D. (2003). Alkenones as paleotemperature indicators. *Treatise on Geochemistry*, 6, 1–44. <https://doi.org/10.1016/B0-08-043751-6/06115-6>
- Hodell, D. A., Channell, J. E. T., Curtis, J. H., Romero, O. E., & Röhl, U. (2008). Onset of “Hudson Strait” Heinrich events in the eastern North Atlantic at the end of the middle Pleistocene transition (~640 ka)? *Paleoceanography*, 23(4), PA4218. <https://doi.org/10.1029/2008PA001591>
- Holte, J., & Talley, L. (2009). A new algorithm for finding mixed layer depths with applications to argo data and subantarctic mode water formation. *Journal of Atmospheric and Oceanic Technology*, 26(9), 1920–1939. <https://doi.org/10.1175/2009JTECHO543.1>
- Hönisch, B., Hemming, N. G., Archer, D., Siddall, M., & McManus, J. F. (2009). Atmospheric carbon dioxide concentration across the mid-Pleistocene transition. *Science*, 324(5934), 1551–1554. <https://doi.org/10.1126/science.1171477>
- Hopmans, E. C., Schouten, S., & Sinninghe Damsté, J. S. (2015). The effect of improved chromatography on GDGT-based palaeoproxies. *Organic Geochemistry*, 93, 1–6. <https://doi.org/10.1016/j.orggeochem.2015.12.006>
- Hopmans, E. C., Weijers, J. W. H., Schefuß, E., Herfort, L., Sinninghe Damsté, J. S., & Schouten, S. (2004). A novel proxy for terrestrial organic matter in sediments based on branched and isoprenoid tetraether lipids. *Earth and Planetary Science Letters*, 224(1–2), 107–116. <https://doi.org/10.1016/j.epsl.2004.05.012>
- Huguet, C., Cartes, J. E., Damsté, J. S. S., & Schouten, S. (2006). Marine crenarchaeotal membrane lipids in decapods: Implications for the TEX86 paleothermometer. *Geochemistry, Geophysics, Geosystems*, 7(11), Q11010. <https://doi.org/10.1029/2006GC001305>
- Huguet, C., Schimmelmann, A., Thunell, R., Lourens, L. J., Damsté, J. S. S., & Schouten, S. (2007). A study of the TEX86 paleothermometer in the water column and sediments of the Santa Barbara Basin, California. *Paleoceanography*, 22(3), PA3203. <https://doi.org/10.1029/2006PA001310>
- Jansen, J. H. F., Kuijpers, A., & Troelstra, S. R. (1986). A mid-brunhes climatic event: Long-term changes in global atmosphere and ocean circulation. *Science*, 232(4750), 619–622. <https://doi.org/10.1126/science.232.4750.619>

- Jouzel, J., Masson-Delmotte, V., Cattani, O., Dreyfus, G., Falourd, S., Hoffmann, G., et al. (2007). Orbital and millennial Antarctic climate variability over the past 800,000 years. *Science*, 317(5839), 793–796. <https://doi.org/10.1126/science.1141038>
- Karner, M. B., DeLong, E. F., & Karl, D. M. (2001). Archaeal dominance in the mesopelagic zone of the Pacific Ocean. *Nature*, 409(6819), 507–510. <https://doi.org/10.1038/35054051>
- Kawamura, K. (1995). Land-derived lipid class compounds in the deep-sea sediments and marine aerosols from North Pacific. *Biogeochemical Processes and Ocean Flux in the Western Pacific*, 31–51.
- Kemp, A. E. S., Grigorov, I., Pearce, R. B., & Naveira Garabato, A. C. (2010). Migration of the Antarctic Polar Front through the mid-Pleistocene transition: Evidence and climatic implications. *Quaternary Science Reviews*, 29(17–18), 1993–2009. <https://doi.org/10.1016/j.quascirev.2010.04.027>
- Kim, J.-H., Huguot, C., Zonneveld, K. A. F., Versteegh, G. J. M., Roeder, W., Sinninghe Damsté, J. S., & Schouten, S. (2009). An experimental field study to test the stability of lipids used for the TEX86 and palaeothermometers. *Geochimica et Cosmochimica Acta*, 73(10), 2888–2898. <https://doi.org/10.1016/j.gca.2009.02.030>
- Kim, J.-H., Schouten, S., Hopmans, E. C., Donner, B., & Sinninghe Damsté, J. S. (2008). Global sediment core-top calibration of the TEX86 paleothermometer in the ocean. *Geochimica et Cosmochimica Acta*, 72(4), 1154–1173. <https://doi.org/10.1016/j.gca.2007.12.010>
- Kim, J.-H., van der Meer, J., Schouten, S., Helmke, P., Willmott, V., Sangiorgi, F., et al. (2010). New indices and calibrations derived from the distribution of crenarchaeal isoprenoid tetraether lipids: Implications for past sea surface temperature reconstructions. *Geochimica et Cosmochimica Acta*, 74(16), 4639–4654. <https://doi.org/10.1016/j.gca.2010.05.027>
- Könneke, M., Bernhard, A. E., de la Torre, J. R., Walker, C. B., Waterbury, J. B., & Stahl, D. A. (2005). Isolation of an autotrophic ammonia-oxidizing marine archaeon. *Nature*, 437(7058), 543–546. <https://doi.org/10.1038/nature03911>
- Lam, P., Jensen, M. M., Lavik, G., McGinnis, D. F., Müller, B., Schubert, C. J., et al. (2007). Linking crenarchaeal and bacterial nitrification to anammox in the Black Sea. *Proceedings of the National Academy of Sciences*, 104(17), 7104–7109. <https://doi.org/10.1073/pnas.0611081104>
- Lawrence, K. T., Herbert, T. D., Brown, C. M., Raymo, M. E., & Haywood, A. M. (2009). High-amplitude variations in North Atlantic sea surface temperature during the early Pliocene warm period. *Paleoceanography*, 24(2), PA2218. <https://doi.org/10.1029/2008PA001669>
- Lear, C. H., Billups, K., Rickaby, R. E. M., Diester-Haass, L., Mawbey, E. M., & Sosdian, S. M. (2016). Breathing more deeply: Deep ocean carbon storage during the mid-Pleistocene climate transition. *Geology*, 44(12), 1035–1038. <https://doi.org/10.1130/G38636.1>
- Lisiecki, L. E. (2010). A benthic  $\delta^{13}\text{C}$ -based proxy for atmospheric  $\text{pCO}_2$  over the last 1.5 Myr. *Geophysical Research Letters*, 37(21), L21708. <https://doi.org/10.1029/2010GL045109>
- Lisiecki, L. E., & Raymo, M. E. (2005). A Pliocene-Pleistocene stack of 57 globally distributed benthic  $\delta^{18}\text{O}$  records. *Paleoceanography*, 20, PA1003. <https://doi.org/10.1029/2004PA001071>
- Llido, J., Garçon, V., Lutjeharms, J. R. E., & Sudre, J. (2005). Event-scale blooms drive enhanced primary productivity at the Subtropical Convergence. *Geophysical Research Letters*, 32(15), L15611. <https://doi.org/10.1029/2005GL022880>
- Lopes dos Santos, R. A., Spooner, M. I., Barrows, T. T., De Deckker, P., Sinninghe Damsté, J. S., & Schouten, S. (2013). Comparison of organic ( $\text{U}_{37}^k$ ,  $\text{TEX}_{86}^h$ , LDI) and faunal proxies (foraminiferal assemblages) for reconstruction of late Quaternary sea surface temperature variability from offshore southeastern Australia: SST from offshore southeastern Australia. *Paleoceanography*, 28(3), 377–387. <https://doi.org/10.1002/palo.20035>
- Lüthi, D., Le Floch, M., Bereiter, B., Blunier, T., Barnola, J.-M., Siegenthaler, U., et al. (2008). High-resolution carbon dioxide concentration record 650,000–800,000 years before present. *Nature*, 453(7193), 379–382. <https://doi.org/10.1038/nature06949>
- Lutjeharms, J. R. E. (2006). *The Agulhas current*. Springer.
- Lutjeharms, J. R. E., & Anson, I. J. (2001). The Agulhas return current. *Journal of Marine Systems*, 30(1–2), 115–138. [https://doi.org/10.1016/S0924-7963\(01\)00041-0](https://doi.org/10.1016/S0924-7963(01)00041-0)
- Lutjeharms, J. R. E., & Valentine, H. R. (1984). Southern Ocean thermal fronts south of Africa. *Deep Sea Research Part A. Oceanographic Research Papers*, 31, 1461–1475. [https://doi.org/10.1016/0198-0149\(84\)90082-7](https://doi.org/10.1016/0198-0149(84)90082-7)
- Maiorano, P., Marino, M., & Flores, J.-A. (2009). The warm interglacial Marine Isotope Stage 31: Evidences from the calcareous nannofossil assemblages at Site 1090 (Southern Ocean). *Marine Micropaleontology*, 71(3–4), 166–175. <https://doi.org/10.1016/j.marmicro.2009.03.002>
- Marino, M., Maiorano, P., Lirer, F., & Pelosi, N. (2009). Response of calcareous nannofossil assemblages to paleoenvironmental changes through the mid-Pleistocene revolution at Site 1090 (Southern Ocean). *Palaeogeography, Palaeoclimatology, Palaeoecology*, 280(3–4), 333–349. <https://doi.org/10.1016/j.palaeo.2009.06.019>
- Martínez-García, A., Rosell-Melé, A., Geibert, W., Gersonde, R., Masqué, P., Gaspari, V., & Barbante, C. (2009). Links between iron supply, marine productivity, sea surface temperature, and  $\text{CO}_2$  over the last 1.1 Ma. *Paleoceanography*, 24(1), PA1207. <https://doi.org/10.1029/2008PA001657>
- Martínez-García, A., Rosell-Melé, A., Jaccard, S. L., Geibert, W., Sigman, D. M., & Haug, G. H. (2011). Southern Ocean dust–climate coupling over the past four million years. *Nature*, 476(7360), 312–315. <https://doi.org/10.1038/nature10310>
- Martínez-Méndez, G., Zahn, R., Hall, I. R., Peeters, F. J. C., Pena, L. D., Cacho, I., & Negre, C. (2010). Contrasting multiproxy reconstructions of surface ocean hydrography in the Agulhas Corridor and implications for the Agulhas Leakage during the last 345,000 years. *Paleoceanography*, 25(4), PA4227. <https://doi.org/10.1029/2009PA001879>
- McClymont, E. L., Sosdian, S. M., Rosell-Melé, A., & Rosenthal, Y. (2013). Pleistocene sea-surface temperature evolution: Early cooling, delayed glacial intensification, and implications for the mid-Pleistocene climate transition. *Earth-Science Reviews*, 123, 173–193. <https://doi.org/10.1016/j.earscirev.2013.04.006>
- Melles, M., Brigham-Grette, J., Minyuk, P. S., Nowaczyk, N. R., Wennrich, V., DeConto, R. M., et al. (2012). 2.8 million years of Arctic climate change from lake El'gygytyn, NE Russia. *Science*, 337(6092), 315–320. <https://doi.org/10.1126/science.1222135>
- Mollenhauer, G., Inthorn, M., Vogt, T., Zabel, M., Damsté, J. S. S., & Eglinton, T. I. (2007). Aging of marine organic matter during cross-shelf lateral transport in the Benguela upwelling system revealed by compound-specific radiocarbon dating. *Geochemistry, Geophysics, Geosystems*, 8(9), Q09004. <https://doi.org/10.1029/2007GC001603>
- Mollenhauer, G., Kienast, M., Lamy, F., Meggers, H., Schneider, R. R., Hayes, J. M., & Eglinton, T. I. (2005). An evaluation of  $^{14}\text{C}$  age relationships between co-occurring foraminifera, alkenones, and total organic carbon in continental margin sediments. *Paleoceanography*, 20(1), PA1016. <https://doi.org/10.1029/2004PA001103>
- Monterey, G. I., & Levitus, S. (1997). Climatological cycle of mixed layer depth in the world ocean, report, 5 pp., NOAA, Silver Spring, Md. In *NOAA Atlas NESDIS 14*, Silver Spring, Md: National Oceanic and Atmospheric Administration.
- Mudelsee, M., & Statteger, K. (1997). Exploring the structure of the mid-Pleistocene revolution with advanced methods of time-series analysis. *Geologische Rundschau*, 86(2), 499–511. <https://doi.org/10.1007/s005310050157>

- Müller, P. J., Kirst, G., Ruhland, G., von Storch, I., & Rosell-Melé, A. (1998). Calibration of the alkenone paleotemperature index based on core-tops from the eastern South Atlantic and the global ocean (60°N–60°S). *Geochimica et Cosmochimica Acta*, 62(10), 1757–1772. [https://doi.org/10.1016/S0016-7037\(98\)00097-0](https://doi.org/10.1016/S0016-7037(98)00097-0)
- Murray, A., Blakis, A., Massana, R., Strawzewski, S., Passow, U., Alldredge, A., & DeLong, E. (1999). A time series assessment of planktonic archaeal variability in the Santa Barbara Channel. *Aquatic Microbial Ecology*, 20, 129–145. <https://doi.org/10.3354/ame020129>
- Naik, D. K., Saraswat, R., Khare, N., Pandey, A. C., & Nigam, R. (2013). Migrating subtropical front and Agulhas Return Current affect the southwestern Indian Ocean during the late Quaternary. *Climate of the Past Discussions*, 9(5), 5521–5551. <https://doi.org/10.5194/cpd-9-5521-2013>
- Ohkouchi, N., Eglinton, T. I., Keigwin, L. D., & Hayes, J. M. (2002). Spatial and temporal offsets between proxy records in a sediment drift. *Science*, 298(5596), 1224–1227. <https://doi.org/10.1126/science.1075287>
- O'Neill, T. A., Hayward, B. W., Kawagata, S., Sabaa, A. T., & Grenfell, H. R. (2007). Pleistocene extinctions of deep-sea benthic foraminifera: The South Atlantic record. *Palaeontology*, 50(5), 1073–1102. <https://doi.org/10.1111/j.1475-4983.2007.00702.x>
- Orsi, A. H., Whitworth, T., & Nowlin, W. D. (1995). On the meridional extent and fronts of the Antarctic Circumpolar Current. *Deep Sea Research Part I: Oceanographic Research Papers*, 42(5), 641–673. [https://doi.org/10.1016/0967-0637\(95\)00021-W](https://doi.org/10.1016/0967-0637(95)00021-W)
- Peeters, F. J. C., Acheson, R., Brummer, G.-J. A., de Ruijter, W. P. M., Schneider, R. R., Ganssen, G. M., et al. (2004). Vigorous exchange between the Indian and Atlantic oceans at the end of the past five glacial periods. *Nature*, 430(7000), 661–665. <https://doi.org/10.1038/nature02785>
- Peña, L. D., & Goldstein, S. L. (2014). Thermohaline circulation crisis and impacts during the mid-Pleistocene transition. *Science*, 345(6194), 318–322. <https://doi.org/10.1126/science.1249770>
- Pépin, L., Raynaud, D., Barnola, J.-M., & Loutre, M. F. (2001). Hemispheric roles of climate forcings during glacial-interglacial transitions as deduced from the Vostok record and LLN-2D model experiments. *Journal of Geophysical Research*, 106(D23), 31885–31892. <https://doi.org/10.1029/2001JD900117>
- Petit, J. R., Jouzel, J., Raynaud, D., Barkov, N. I., Delaygue, G., Delmotte, M., et al. (1999). Climate and atmospheric history of the past 420,000 years from the Vostok ice core, Antarctica. *Nature*, 399, 429–436. <https://doi.org/10.1038/20859>
- Petrick, B., McClymont, E. L., Littler, K., Rosell-Melé, A., Clarkson, M. O., Maslin, M., et al. (2018). Oceanographic and climatic evolution of the southeastern subtropical Atlantic over the last 3.5 Ma. *Earth and Planetary Science Letters*, 492, 12–21. <https://doi.org/10.1016/j.epsl.2018.03.054>
- Pollard, D., & DeConto, R. M. (2009). Modeling West Antarctic ice sheet growth and collapse through the past five million years. *Nature*, 458(7236), 329–332. <https://doi.org/10.1038/nature07809>
- Pollard, R. T., Lucas, M. I., & Read, J. F. (2002). Physical controls on biogeochemical zonation in the Southern Ocean. *Deep Sea Research Part II: Topical Studies in Oceanography*, 49(16), 3289–3305. [https://doi.org/10.1016/S0967-0645\(02\)00084-X](https://doi.org/10.1016/S0967-0645(02)00084-X)
- Prahl, F. G., & Wakeham, S. G. (1987). Calibration of unsaturation patterns in long-chain ketone compositions for palaeotemperature assessment. *Nature*, 330(6146), 367–369. <https://doi.org/10.1038/330367a0>
- Qin, W., Carlson, L. T., Armbrust, E. V., Devol, A. H., Moffett, J. W., Stahl, D. A., & Ingalls, A. E. (2015). Confounding effects of oxygen and temperature on the TEX<sub>86</sub> signature of marine Thaumarchaeota. *Proceedings of the National Academy of Sciences*, 112(35), 10979–10984. <https://doi.org/10.1073/pnas.1501568112>
- Ravelo, A. C., Andreasen, D. H., Lyle, M., Olivarez Lyle, A., & Wara, M. W. (2004). Regional climate shifts caused by gradual global cooling in the Pliocene epoch. *Nature*, 429(6989), 263–267. <https://doi.org/10.1038/nature02567>
- Raymo, M. E., Lisiecki, L. E., & Nisancioglu, K. H. (2006). Plio-Pleistocene ice volume, Antarctic climate, and the global δ<sup>18</sup>O record. *Science*, 313(5786), 492–495. <https://doi.org/10.1126/science.1123296>
- Raymo, M. E., Oppo, D. W., & Curry, W. (1997). The Mid-Pleistocene climate transition: A deep sea carbon isotopic perspective. *Paleoceanography*, 12(4), 546–559. <https://doi.org/10.1029/97PA01019>
- Raynaud, D., Barnola, J.-M., Souchez, R., Lorrain, R., Petit, J.-R., Duval, P., & Lipenkov, V. Y. (2005). Palaeoclimatology: The record for marine isotopic stage 11. *Nature*, 436(7047), 39–40. <https://doi.org/10.1038/43639b>
- Read, J. F., Lucas, M. I., Holley, S. E., & Pollard, R. T. (2000). Phytoplankton, nutrients and hydrography in the frontal zone between the Southwest Indian Subtropical gyre and the Southern Ocean. *Deep Sea Research Part I: Oceanographic Research Papers*, 47(12), 2341–2367. [https://doi.org/10.1016/S0967-0637\(00\)00021-2](https://doi.org/10.1016/S0967-0637(00)00021-2)
- Romero, O. E., Kim, J.-H., Bárcena, M. A., Hall, I. R., Zahn, R., & Schneider, R. (2015). High-latitude forcing of diatom productivity in the southern Agulhas Plateau during the past 350 kyr: Late Pleistocene diatom productivity. *Paleoceanography*, 30(2), 118–132. <https://doi.org/10.1002/2014PA002636>
- Rosell-Melé, A., Martínez-García, A., & McClymont, E. L. (2014). Persistent warmth across the Benguela upwelling system during the Pliocene epoch. *Earth and Planetary Science Letters*, 386, 10–20. <https://doi.org/10.1016/j.epsl.2013.10.041>
- Rosell-Melé, A., Maslin, M. A., Maxwell, J. R., & Schaeffer, P. (1997). Biomarker evidence for “Heinrich” events. *Geochimica et Cosmochimica Acta*, 61(8), 1671–1678. [https://doi.org/10.1016/S0016-7037\(97\)00046-X](https://doi.org/10.1016/S0016-7037(97)00046-X)
- Schefuß, E., Sinninghe Damsté, J. S., & Jansen, J. H. F. (2004). Forcing of tropical Atlantic sea surface temperatures during the mid-Pleistocene transition. *Paleoceanography*, 19(4), PA4029. <https://doi.org/10.1029/2003PA000892>
- Scherer, R. P., Bohaty, S. M., Dunbar, R. B., Esper, O., Flores, J.-A., Gersonde, R., et al. (2008). Antarctic records of precession-paced insolation-driven warming during early Pleistocene Marine Isotope Stage 31. *Geophysical Research Letters*, 35(3). <https://doi.org/10.1029/2007GL032254>
- Schlitzer, R. (2014). *Ocean data view*. Retrieved from <http://odv.awi.de>
- Schmieder, F., von Döbenek, T., & Bleil, U. (2000). The Mid-Pleistocene climate transition as documented in the deep South Atlantic Ocean: Initiation, interim state and terminal event. *Earth and Planetary Science Letters*, 179(3), 539–549. [https://doi.org/10.1016/S0012-821X\(00\)00143-6](https://doi.org/10.1016/S0012-821X(00)00143-6)
- Schouten, S., Hoppmans, E. C., Schefuß, E., & Sinninghe Damsté, J. S. (2002). Distributional variations in marine crenarchaeotal membrane lipids: A new tool for reconstructing ancient sea water temperatures? *Earth and Planetary Science Letters*, 204(1–2), 265–274. [https://doi.org/10.1016/S0012-821X\(02\)00979-2](https://doi.org/10.1016/S0012-821X(02)00979-2)
- Schouten, S., Hoppmans, E. C., & Sinninghe Damsté, J. S. (2004). The effect of maturity and depositional redox conditions on archaeal tetraether lipid palaeothermometry. *Organic Geochemistry*, 35(5), 567–571. <https://doi.org/10.1016/j.orggeochem.2004.01.012>
- Schouten, S., Hoppmans, E. C., & Sinninghe Damsté, J. S. (2013). The organic geochemistry of glycerol dialkyl glycerol tetraether lipids: A review. *Organic Geochemistry*, 54, 19–61. <https://doi.org/10.1016/j.orggeochem.2012.09.006>
- Sexton, P. F., & Norris, R. D. (2011). High latitude regulation of low latitude thermocline ventilation and planktic foraminifer populations across glacial–interglacial cycles. *Earth and Planetary Science Letters*, 311(1–2), 69–81. <https://doi.org/10.1016/j.epsl.2011.08.044>

- Shah, S. R., Mollenhauer, G., Ohkouchi, N., Eglinton, T. I., & Pearson, A. (2008). Origins of archaeal tetraether lipids in sediments: Insights from radiocarbon analysis. *Geochimica et Cosmochimica Acta*, 72(18), 4577–4594. <https://doi.org/10.1016/j.gca.2008.06.021>
- Sikes, E. L., Howard, W. R., Neil, H. L., & Volkman, J. K. (2002). Glacial-interglacial sea surface temperature changes across the subtropical front east of New Zealand based on alkenone unsaturation ratios and foraminiferal assemblages. *Paleoceanography*, 17(2), 2–13. <https://doi.org/10.1029/2001PA000640>
- Simon, M. H., Arthur, K. L., Hall, I. R., Peeters, F. J. C., Loveday, B. R., Barker, S., et al. (2013). Millennial-scale Agulhas Current variability and its implications for salt-leakage through the Indian–Atlantic Ocean Gateway. *Earth and Planetary Science Letters*, 383, 101–112. <https://doi.org/10.1016/j.epsl.2013.09.035>
- Simoneit, B. R. T. (1977). Organic matter in eolian dusts over the Atlantic Ocean. *Marine Chemistry*, 5(4–6), 443–464. [https://doi.org/10.1016/0304-4203\(77\)90034-2](https://doi.org/10.1016/0304-4203(77)90034-2)
- Stahl, D. A., & de la Torre, J. R. (2012). Physiology and diversity of ammonia-oxidizing archaea. *Annual Review of Microbiology*, 66(1), 83–101. <https://doi.org/10.1146/annurev-micro-092611-150128>
- Starr, A., Hall, I. R., Barker, S., Rackow, T., Zhang, X., Hemming, S. R., et al. (2021). Antarctic icebergs reorganize ocean circulation during Pleistocene glacials. *Nature*, 589(7841), 236–241. <https://doi.org/10.1038/s41586-020-03094-7>
- Stewart, F. J., Ulloa, O., & DeLong, E. F. (2012). Microbial metatranscriptomics in a permanent marine oxygen minimum zone: OMZ community gene expression. *Environmental Microbiology*, 14(1), 23–40. <https://doi.org/10.1111/j.1462-2920.2010.02400.x>
- Stramma, L., & Peterson, R. G. (1990). The South Atlantic current. *Journal of Physical Oceanography*, 20(6), 846–859. [https://doi.org/10.1175/1520-0485\(1990\)020<0846:TSAC>2.0.CO;2](https://doi.org/10.1175/1520-0485(1990)020<0846:TSAC>2.0.CO;2)
- Tece, M. A., Getliff, J. M., Leftley, J. W., Parkes, R. J., & Maxwell, J. R. (1998). Microbial degradation of the marine prymnesiophyte *Emiliana huxleyi* under oxic and anoxic conditions as a model for early diagenesis: Long chain alkadienes, alkenones and alkyl alkenoates. *Organic Geochemistry*, 29(4), 863–880. [https://doi.org/10.1016/S0146-6380\(98\)00145-4](https://doi.org/10.1016/S0146-6380(98)00145-4)
- Teitler, L., Florindo, F., Warnke, D. A., Filippelli, G. M., Kupp, G., & Taylor, B. (2015). Antarctic Ice Sheet response to a long warm interval across Marine Isotope Stage 31: A cross-latitudinal study of iceberg-rafted debris. *Earth and Planetary Science Letters*, 409, 109–119. <https://doi.org/10.1016/j.epsl.2014.10.037>
- Tierney, J. E., & Tingley, M. P. (2014). A Bayesian, spatially-varying calibration model for the TEX<sub>86</sub> proxy. *Geochimica et Cosmochimica Acta*, 127, 83–106. <https://doi.org/10.1016/j.gca.2013.11.026>
- Tierney, J. E., & Tingley, M. P. (2015). A TEX<sub>86</sub> surface sediment database and extended Bayesian calibration. *Scientific Data*, 2, 150029. <https://doi.org/10.1038/sdata.2015.29>
- Toggweiler, J. R., Russell, J. L., & Carson, S. R. (2006). Midlatitude westerlies, atmospheric CO<sub>2</sub>, and climate change during the ice ages. *Paleoceanography*, 21(2), PA2005. <https://doi.org/10.1029/2005PA001154>
- Volkman, J. K., Eglinton, G., Corner, E. D. S., & Forsberg, T. E. V. (1980). Long-chain alkenes and alkenones in the marine coccolithophorid *Emiliana huxleyi*. *Phytochemistry*, 19(12), 2619–2622. [https://doi.org/10.1016/S0031-9422\(00\)83930-8](https://doi.org/10.1016/S0031-9422(00)83930-8)
- Wakeham, S. G., Amann, R., Freeman, K. H., Hopmans, E. C., Jørgensen, B. B., Putnam, I. F., et al. (2007). Microbial ecology of the stratified water column of the Black Sea as revealed by a comprehensive biomarker study. *Organic Geochemistry*, 38(12), 2070–2097. <https://doi.org/10.1016/j.orggeochem.2007.08.003>
- Weijer, W. (2002). Response of the Atlantic overturning circulation to South Atlantic sources of buoyancy. *Global and Planetary Change*, 34(3–4), 293–311. [https://doi.org/10.1016/S0921-8181\(02\)00121-2](https://doi.org/10.1016/S0921-8181(02)00121-2)
- Whitworth, T., & Nowlin, W. D. (1987). Water masses and currents of the Southern Ocean at the Greenwich Meridian. *Journal of Geophysical Research*, 92(C6), 6462. <https://doi.org/10.1029/JC092iC06p06462>
- Wuchter, C., Schouten, S., Wakeham, S. G., & Damsté, J. S. S. (2005). Temporal and spatial variation in tetraether membrane lipids of marine Crenarchaeota in particulate organic matter: Implications for TEX<sub>86</sub> paleothermometry. *Paleoceanography*, 20(3), PA3013. <https://doi.org/10.1029/2004PA001110>

## References From the Supporting Information

- Zhang, Y. G., Pagani, M., & Wang, Z. (2016). Ring Index: A new strategy to evaluate the integrity of TEX<sub>86</sub> paleothermometry. *Paleoceanography*, 31(2), 220–232. <https://doi.org/10.1002/2015PA002848>
- Zhang, Y. G., Zhang, C. L., Liu, X.-L., Li, L., Hinrichs, K.-U., & Noakes, J. E. (2011). Methane Index: A tetraether archaeal lipid biomarker indicator for detecting the instability of marine gas hydrates. *Earth and Planetary Science Letters*, 307(3–4), 525–534. <https://doi.org/10.1016/j.epsl.2011.05.031>